Received: 3 February 2021 | Revised: 19 May 2021 | Accepted: 20 May 2021

DOI: 10.1002/qj.4114

Quarterly Journal of the Royal Meteorological Society RMetS

RESEARCH ARTICLE

Distilling the mechanism for the Madden–Julian Oscillation into a simple translating structure

Geoffrey K. Vallis

Department of Mathematics, University of Exeter, Exeter, UK

Correspondence
G. K. Vallis, Department of Mathematics, University of Exeter, Exeter EX4 4QF, UK.
Email: g.vallis@exeter.ac.uk

Funding information
U.K. NERC under the ParaCon project.
The Newton Fund under the Weather and Climate Science for Services Partnership

Abstract

This article presents a minimal model of the Madden–Julian Oscillation (MJO), isolating a robust mechanism that leads to the observed characteristic pattern and eastward propagation. A localized heat source at the Equator leads to a Gill-like pattern in the geopotential, with moist air converging toward the heat source. Over a fairly wide range of parameters, the moisture convergence is found to be slightly to the east of the heat source, with moist air advected in from the east along the Kelvin lobe meeting slightly drier air advected meridionally around the Rossby lobes. The associated condensation then gives rise to a heat source that also is east of the original one, thus causing the pattern itself to propagate east with dryer regions both to the east and west of the region of precipitation. The speed of the propagation is limited by the ability of the moisture advection to move the condensational heat source; it thus scales with the fluid speed which is induced by the convective heat source, and so with the strength of the convective heating, and not with a gravity wave speed. The propagation speed also increases with the nominal offset between the centre of the pattern and the subsequent moistening and condensation. In the real world this distance, as well as the level and coherence of condensation, are determined not only by the location of moisture convergence but also by the complex physics of convection in the tropical environment. Thus, even though the underlying MJO mechanism is itself not complicated, its reproduction will depend rather sensitively on model parameters in simulations with comprehensive numerical models.

KEYWORDS

convection, Madden–Julian Oscillation, tropical dynamics

1 | INTRODUCTION

The Madden–Julian Oscillation (MJO) is, as is well known, a large-scale precipitating disturbance centred near the Equator, extending meridionally to about 20° North and South and with an influence in the geopotential and velocity fields that extends many thousands of kilometres. The disturbance typically forms over the warm waters of the Indian Ocean and propagates eastward with a speed of around $5\,\mathrm{m\cdot s^{-1}}$, passing over the Maritime Continent

and decaying over the cooler waters of the eastern equatorial Pacific. The disturbance may reform some tens of days later and the phenomenon repeats – hence it has become known as an oscillation, although in many respects it better resembles a translating disturbance. The phenomenon was described by Madden and Julian (1971) and reviews and discussions of various observations and processes have been given by Zhang (2005), Lau and Waliser (2012), DeMott *et al.* (2015) and others.

In addition to analyses of the observations, attempts to understand the MJO have largely proceeded along two tracks. One is via the use of three-dimensional models, either General Circulation Models (GCMs) with parametrized convection or, more recently, near-Cloud Resolving Models (CRMs) which attempt to resolve or at least represent convection without parametrization (e.g., Liu *et al.*, 2009; Nasuno *et al.*, 2009; Holloway *et al.*, 2013; Arnold and Randall, 2015; Khairoutdinov and Emanuel, 2018). However, many comprehensive models still have trouble reproducing the phenomenon. In the second, more theoretical, track, much simpler models of equatorial dynamics are employed, often centred around the shallow-water equations or variations thereof, with some treatment of moisture (e.g., Yano *et al.*, 1995; Raymond and Fuchs, 2009; Sobel and Maloney, 2013; Fuchs and Raymond, 2017; Vallis and Penn, 2020). It is the second track that we follow here, but we are much influenced by the phenomenology emerging from observations and experiments with more comprehensive numerical models.

Our goal in this paper is not to produce a complete mathematical theory of the MJO (and for reasons that will become clear, we do not believe that is possible except in a qualitative sense). Rather, it is to present a minimal model that distills the mechanism to a core and explains the large-scale patterns in geopotential and precipitation, providing a simple mechanism for eastward propagation and a scaling for its speed. In spite of the simplicity of explanation, the model also suggests why it is that comprehensive models often have difficulty in simulating the phenomenon. The model draws in part on previous work by Vallis and Penn (2020), an article that presents a model with more complicated behaviour. Here we simplify that model and keep only aspects essential to the phenomenon. We try to make this article self-contained, necessitating a small amount of duplication in Sections 2 and 3.

In the following section we summarize the essential phenomenology of the MJO. We then describe the mechanism we are putting forward, and describe various numerical experiments illustrating it. We then describe its relation to observations and various other models, and finally we give some summary remarks.

2 | MAIN FEATURES OF THE MJO

Observations, reanalyses, and numerical experiments with comprehensive numerical models reveal several robust features of the MJO.

1. The defining feature is a precipitation pattern centred around the Equator, propagating east at a few metres per second, although the speed varies somewhat from event to event (Madden and Julian, 1971; 1972). This relatively slow speed gives it a spectral signature that differentiates it from a faster moving Kelvin wave (Wheeler and Kiladis, 1999).
2. The large-scale horizontal structure in the pressure or geopotential field resembles, after some filtering or composite-averaging, a Matsuno–Gill pattern, albeit with differences in shape and extent depending on the details of analysis (Kiladis *et al.*, 2005, and others).
3. The vertical structure of MJO can be largely represented by a deep, first-baroclinic mode, with smaller barotropic and higher-order baroclinic fields (Sperber, 2003; Kiladis *et al.*, 2005).
4. Overall, diabatic heating in the MJO is dominated by latent heat release (Jiang *et al.*, 2011; Adames and Wallace, 2015), although radiative effects can be significant.
5. The moisture source for the precipitation is convergence in the lower atmosphere, not local evaporation (de Szoeke *et al.*, 2015). Furthermore, there is an east–west asymmetry in the boundary-layer moisture budget, with a low-level moistening ahead of (i.e., east of) the main convection zone (Hsu and Li, 2012; Jiang *et al.*, 2015; de Szoeke and Maloney, 2020). The humidity and precipitation anomalies are also strongest slightly to the east of the centre of the pattern, albeit with some differences between reanalysis products and observations (e.g., Mapes and Bacmeister, 2012; Adames and Wallace, 2015).

A slew of other more detailed properties of the MJO have been identified by various investigators, some more robust than others. These include the various phases of the MJO as it traverses across the ocean (Wheeler and Hendon, 2004), a secondary quadrupole structure in the horizontal, the influence of the seasonal cycle and intra- and inter-seasonal irregularity, the interaction with the Asian monsoon, and various associated multi-scale features (e.g., smaller-scale convective events surrounding the main precipitating region). Some of these are addressed in (Vallis and Penn, 2020), but in this article we focus on the topics in the itemized list above.

Of the above listed characteristics, the vertical structure largely follows from the effects of moist convection and associated adjustment processes, maintaining a quasi-equilibrium with a saturated adiabatic lapse rate through the troposphere. In the horizontal, Matsuno–Gill patterns arise when there is a source of heating at or near the Equator (Matsuno, 1966; Gill, 1980), and in the Gill problem specifically there is (in the canonical symmetric case) a stationary localized heat source at the Equator. Note, though, that the MJO is a *moving* pattern, so cannot be precisely a Gill pattern. The heat source in the MJO problem can be associated with the latent heat release by localized precipitation and thus the production of Gill-like patterns is not particularly mysterious; rather, the question is why and at what speed does that pattern move east.

A model of the phenomenon that produced the eastward propagation (and other variability) was offered in Vallis and Penn (2020) using the moist shallow-water equations. Evaporation from the surface provided moisture, which was then advected around and removed when the fluid became saturated. Condensation at or near the Equator produced a Gill-like pattern, with convergence drawing more moisture in to the convection zone and so sustaining the disturbance. Over a fairly wide range of parameters, the ensuing convection occurred just east of the centre of the existing pattern, generating in turn a Gill-like pattern east of the existing one. In certain circumstances this process was self-sustaining, producing an eastward-propagating precipitating disturbance.

In this article we further simplify that model and eliminate all variability except that associated with the moving pattern itself, and thereby identify an unambiguous mechanism for the generation of the pattern and its eastward movement. We find that a fairly generic property of Gill-like patterns is that moisture convergence is offset slightly to the east of the centre of the pattern (the centre being determined by the location of the initial heating). The associated convection provides a condensational heat source that sustains the convergence, with its offset from the initial heating then shifting the entire pattern east; the process repeats, and eastward propagation ensues. The speed of the propagation scales with the fluid speed that is produced by the condensational heating, not with a gravity wave speed. Let us begin our description of all this with the equations of motion.

3 | THE MOIST SHALLOW-WATER EQUATIONS

The vertical structure of the tropical atmosphere has a relatively simple structure which can be reasonably well represented by the first baroclinic mode. If nonlinearities are weak in the momentum equations, the primitive equations then approximately reduce to the shallow-water equations (Matsuno, 1966; McCreary, 1981; Vallis, 2017). The addition of an evolution equation for moisture in the lower atmosphere then gives the moist shallow-water equations and these are, in dimensional notation and without any dissipative terms,

$$\frac{\partial \boldsymbol{u}}{\partial t} + \boldsymbol{f} \times \mathbf{u} = -g\nabla h, \tag{1a}$$

$$\frac{\partial h}{\partial t} + H\nabla \cdot \mathbf{u} = Q_R + Q_L \tag{1b}$$

$$\frac{\partial q}{\partial t} + \nabla \cdot (q\mathbf{u}) = E - C. \tag{1c}$$

The equations are to be solved on an equatorial beta plane with $\boldsymbol{f} = (f_0 + \beta y)\widehat{\mathbf{k}}$, q is a specific humidity, E represents evaporation, C represents condensation, Q_R is the diabatic heating due to radiative effects and Q_L represents the latent heat release due to condensation, and other notation is standard for the shallow-water equations.

The momentum and height equations have been linearized about a state of rest so that H is the depth of the basic state and h is the deviation from this. The release of latent heat Q_L may be related to condensation by $Q_L = -\gamma C$ where γ is a latent heat of condensation. The radiative damping, Q_R, is taken as a relaxation back to a flat height field on a time-scale of several days. Frictional effects are included by the addition of a drag in the momentum equation but no separate boundary layer is included. Related equations have previously been presented by Yano *et al.* (1995), Bouchut *et al.* (2009), Sukhatme (2014), Majda and Stechmann (2009) and Vallis and Penn (2020), and more generally the use of equations that arise from a severe vertical truncation is a common feature of studies in tropical meteorology.

One simple recipe for condensation is to assume that it occurs on saturation, so relaxing the moisture back to the saturation level. This may be represented by

$$C = \begin{cases} (q - q_s)/\tau & q > q_s, \\ 0 & q \le q_s, \end{cases} \tag{2}$$

where q_s is the saturation specific humidity and τ is a specified time-scale (discussed later). The saturation specific humidity may be taken as an increasing function of temperature (a consequence of the Clausius–Clapeyron relation) and we may represent that as an exponential function of the height field,

$$q_s = q_0 \exp(-\alpha h), \tag{3}$$

where α is a constant (which may be zero, in which case q_s is a constant). Evaporation from the surface is represented as

$$E = \begin{cases} C_q(q_g - q) & q_g > q, \\ 0 & q_g \le q, \end{cases} \tag{4}$$

where C_q and q_g are constants or potentially a function of velocity. Vallis and Penn (2020) give a more detailed description of all these terms. In the rest of the article we non-dimensionalize lengths by the equatorial deformation radius $(c/2\beta)^{1/2}$, time by the factor $(2c\beta)^{-1/2}$ and velocities by c, where $c = \sqrt{gH}$. We will also refer to the geopotential, $\phi = gh$, which is proportional to pressure.

The above set of equations has no explicit representation of the boundary layer, although frictional convergence does occur though the addition of a Rayleigh drag in the momentum equations. Clearly the equations are a simplification of the tropical atmosphere but nevertheless capture the main aspects of the interaction of moisture and the dynamical fields in a transparent way.

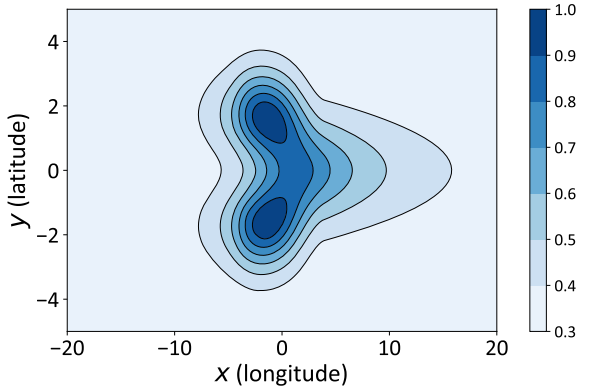

FIGURE 1 Saturated moisture field, q_s, as given by (5) with $\alpha = 0.5$, scaled by its maximum value, associated with the Gill solution with a heat source of amplitude unity centred at (0,0). The horizontal axes (here and in subsequent figures) are scaled by the equatorial deformation radius and the Equator is at $y = 0$ [Colour figure can be viewed at wileyonlinelibrary.com]

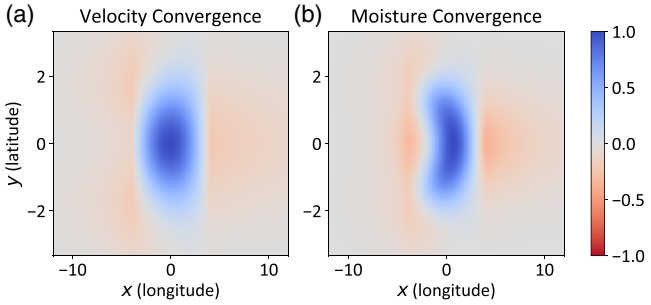

FIGURE 2 Convergence of (a) velocity, $-\nabla \cdot \mathbf{u}$, and (b) the saturated value of moisture $-\nabla \cdot (\mathbf{u}q_s)$ in the Gill solution. Both fields are normalized by their maximum value, and the horizontal axes are scaled by the equatorial deformation radius. The velocity convergence is centred on the point (0,0) whereas the moisture convergence is east of that, as seen clearly in Figure 3 [Colour figure can be viewed at wileyonlinelibrary.com]

4 | HUMIDITY IN THE GILL SOLUTION

4.1 | Moisture convergence in the Gill solution

Let us first suppose that the velocity and geopotential fields are given by the canonical Gill solution itself, the analytic expressions for which are given in the Appendix, with Gill's canonical relaxation constant $\epsilon = 0.1$ used for linear damping of both momentum and geopotential. Suppose also (for now) that the atmosphere has a constant relative humidity (which can be taken to be unity) so that

$$q = q_0 \exp(-\alpha \phi_G), \tag{5}$$

where ϕ_G is given by (A1) and we rescale α from (3). This specific humidity field, shown in Figure 1 has a similar structure to the Gill pattern itself. However, the humidity convergence differs slightly from the velocity convergence as illustrated in Figures 2 and 3: specifically, the centre of moisture convergence is slightly to the east of the heating source that provides the pattern in the first instance, and in this case the distance is about one equatorial deformation radius.

4.1.1 | Evolving the moisture

A similar result regarding the humidity convergence holds if we numerically integrate the moist shallow-water equations, that is, Equations (1)–(4), forward in time, without any assumption of constant relative humidity. In this and subsequent numerical experiments, we solve the equations in a periodic channel of size 40×10 deformation radii, using a uniform grid with 500 grid points in the x-direction corresponding to a grid size of 0.08 deformation radii (or about 80 km), and similarly in the y-direction, using Adams–Bashforth third-order timestepping.

In the first instance we force the equations with stationary localized heat source at the Equator independent of the moisture field, and treat moisture as a passive tracer. The pressure and velocity fields then evolve into a familiar Gill-like pattern. The moisture now enters the system by evaporation, is advected around and condenses upon saturation, and the convergence of velocity and the condensation itself in two representative solutions are shown

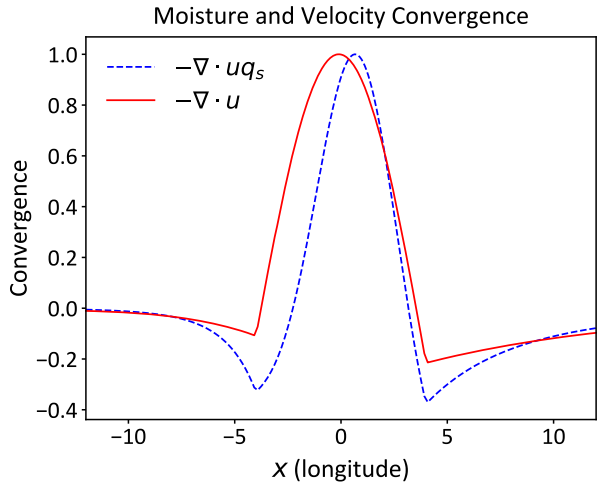

FIGURE 3 As Figure 2, but now showing convergence of velocity, $-\nabla \cdot \mathbf{u}$ (solid red curve), and the saturated specific humidity, $-\nabla \cdot (\mathbf{u}q_s)$ (blue dotted curve) at the Equator. Both fields are normalized by their maximum value [Colour figure can be viewed at wileyonlinelibrary.com]

in Figure 4. In one case the saturation specific humidity varies exponentially with temperature and, at each timestep, all the humidity that exceeds the saturation value is removed (the so-called fast condensation limit). In the other case the saturation specific humidity is set to a constant and the moisture condensation time-scale is several hours (much longer that an single timestep), more in line with the empirical guidelines suggested in Bretherton *et al.* (2004). In both cases the condensation forms east of the centre of the pattern, which is where the heating is located and where the velocity convergence is largest. The precipitation is also largest where the humidity itself is largest (broadly consistent with Bretherton *et al.*, 2004 and Holloway and Neelin 2009), with dry regions to either side. If the saturation specific humidity is constant, then in the fast condensation limit there is no eastward offset (and thus no propagating MJO). This is because the specific humidity is then virtually constant over the region of convergence, and then the moisture convergence is coincidental with the velocity convergence.

The supply of moisture for the precipitation is effected by a flux of moisture from the east meeting slightly dryer air advected from the west and meridionally around the Rossby lobes, as shown in Figure 5 (and again schematically in Figure 12). The moisture convergence is noticeably east of the heat source, by about a deformation radius in these cases. The general nature of these results are not especially sensitive to the parameters chosen to represent evaporation or frictional drag in the equations of motion, nor to the particular form of heating used to produce the pattern. In Figure 4 a heating pattern similar to that of the original Gill problem was used. If we use either a meridionally extended diabatic heating pattern, which stretches several deformation radii north and south, or a zonally extended pattern, a similar result emerges. We explore this further later on, and the reader may look ahead to Figure 8.

Let us now suppose that, instead of being imposed, the heat source producing the pressure pattern is that produced by the condensation itself. Then, since the heating is east of the original source, the system will be pulled toward the new source by the pressure field, shifting the condensation eastward; the process repeats and a continuous eastward propagation ensues. Before showing this result in the shallow-water equations, we illustrate the process with a simple but informative toy model.

5 | A TOY MODEL OF EASTWARD PROPAGATION

Let us represent the Gill solution interacting with an interacting moisture field by a pair of ordinary differential equations with just two independent variables: X_P, the position of the centre of the pattern of the pressure field and X_C, the position of the condensation. We suppose that the condensation provides a heat source toward which the pattern is drawn, and specifically that X_P is drawn towards

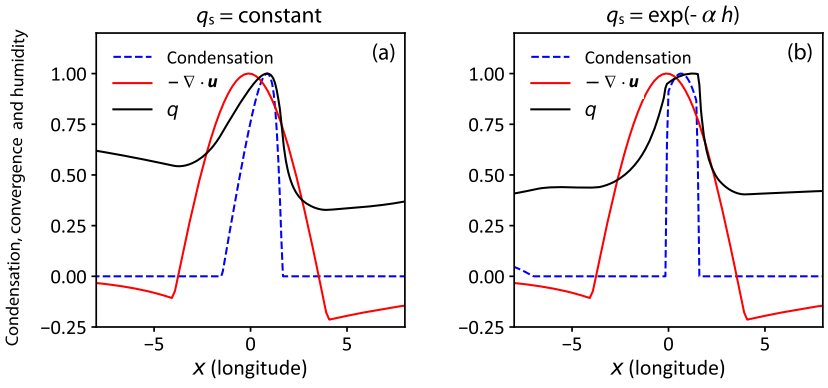

FIGURE 4 The condensation, velocity convergence and humidity in numerical solutions of the moist shallow-water equations with a specified, stationary, heat source centred at $x = 0$. All fields are normalized by their maximum values. In (a) the saturation specific humidity is constant and the condensation time-scale τ is (when dimensionalised) several hours. In (b) the saturation specific humidity varies as in Figure 1 and excess moisture is removed immediately on saturation [Colour figure can be viewed at wileyonlinelibrary.com]

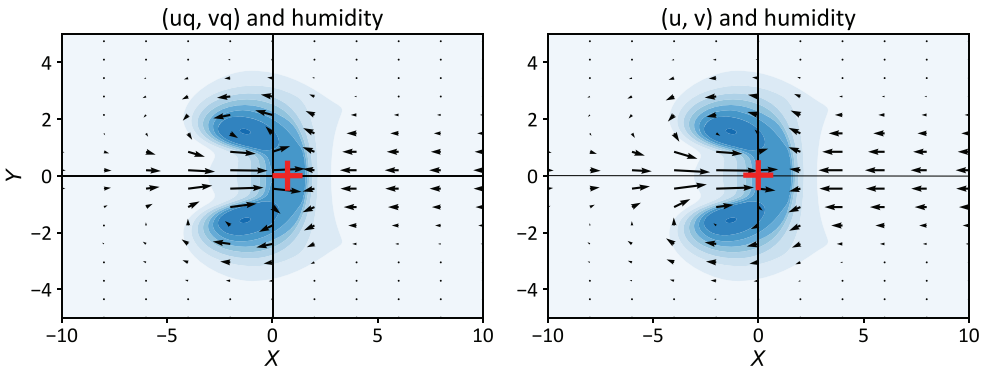

FIGURE 5 (a) The flux of moisture ($\mathbf{u}q$, arrows) and (b) the velocity ($\mathbf{u}$, arrows) superimposed on the moisture field (colour shading, both panels), from the solution in Figure 4b. (A similar result holds for the solution in Figure 4a.) The location of the maximum convergence in each case (i.e., of $-\nabla\cdot(\mathbf{u}q)$ and $-\nabla\cdot\mathbf{u}$) is marked with a red cross [Colour figure can be viewed at wileyonlinelibrary.com]

X_C at a rate k_1. To represent this we write

$$\frac{\mathrm{d}X_P}{\mathrm{d}t} = k_1(X_C - X_P). \tag{6a}$$

The constant k_1 represents the rate of adjustment of the centre of pressure field (and hence also the velocity field) to a condensational heat source located at X_C. Thus, k_1 may be taken to be proportional to a gravity wave speed divided by a length-scale.

We saw earlier that the condensation in the moist shallow-water equation is drawn to a position that is offset from the centre of the pattern, and let this offset be ΔX (see also Figure 12b below). The effect may then be represented by supposing that the centre of the condensation, X_C, is drawn toward the position $X_P + \Delta X$ at a rate k_2 so that

$$\frac{\mathrm{d}X_C}{\mathrm{d}t} = k_2\left([X_P + \Delta X] - X_C\right). \tag{6b}$$

Unlike the pressure field, the moisture evolves advectively so that k_2 is proportional to the fluid speed divided by a length-scale. In most tropical situations the fluid speed ($\sim 5\,\mathrm{m\cdot s^{-1}}$) is much less than the gravity wave speed ($\sim 20\,\mathrm{m\cdot s^{-1}}$) and therefore $k_2 \ll k_1$.

The solution of the above two equations, after an initial transient has died, is

$$X_P = X_0 + \frac{k_1 k_2 \Delta X}{k_1 + k_2} t, \tag{7}$$

where X_0 is a constant, and similarly for X_C. The positions of the condensation and centre of the pressure pattern are then related by

$$X_C - X_P = \frac{k_2 \Delta X}{k_1 + k_2}. \tag{8}$$

Two limiting cases are particularly informative. If $k_2 \gg k_1$ then $X_C \approx X_P + \Delta X$ and (6a) becomes $\mathrm{d}X_P/\mathrm{d}t = k_1\Delta X$, and the entire system propagates east at a speed $k_1\Delta X$. If $k_2 \ll k_1$ then $X_C \approx X_P$ and (6b) becomes $\mathrm{d}X_C/\mathrm{d}t = k_2\Delta X$, and the system also propagates east, but now at a speed $k_2\Delta X$ and with the centre of the pressure almost coincident with the condensation. It is the second limit that is more relevant in the MJO case, since as noted the moisture convergence forms on a slow advective time-scale whereas the pressure pattern forms on a time-scale determined by the faster gravity wave speed. In both cases, though, the speed is proportional to the nominal offset, ΔX, between the centre of the pattern and the position to which the condensation is drawn. That distance cannot be accurately determined by a simple model, or even the full moist shallow-water equations, since it depends on details of convection and radiation. This fact precludes formulating an MJO theory that is both simple and quantitatively accurate; indeed, since precipitation is one of the most difficult quantities for comprehensive models to properly predict, it suggests why those models do not always faithfully reproduce MJO events.

6 | INTEGRATIONS OF THE EQUATIONS OF MOTION

We now describe results arising from various numerical integrations of the shallow-water equations. We begin by using the dry equations to explore how the Gill solution changes when the heating source moves.

6.1 | Dry equations with a localized, moving heat source

We numerically integrate the dry shallow-water equations (i.e., (1)a, b) with a localised heating source at the Equator. The heating source is specified to be that in the Gill problem except that we move it eastward at a specified

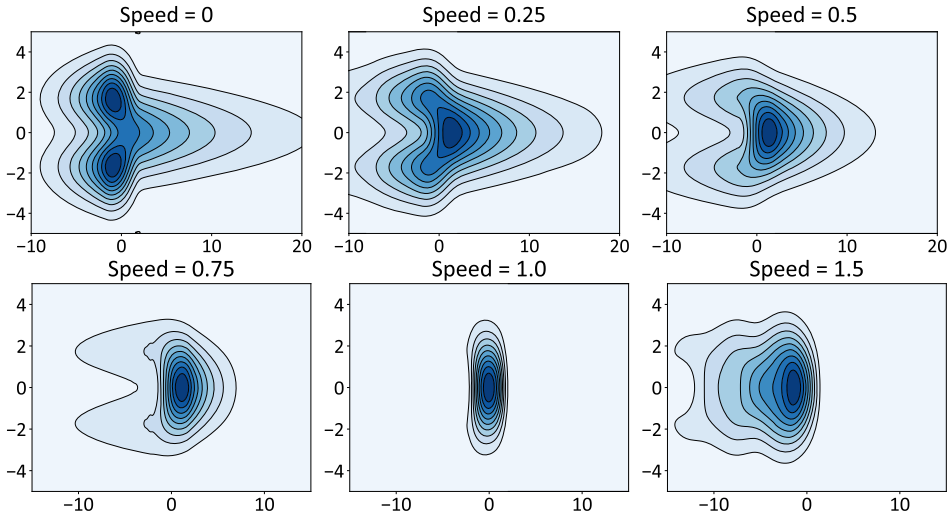

FIGURE 6 Pressure field in solutions of the shallow-water equations with a moving heat source. The x and y co-ordinates are scaled by the deformation radius and the speed is scaled by the gravity wave speed. The heat source is localized at the Equator, with a horizontal scale of about two deformation radii, and moves eastward at a constant speed. For plotting purposes the x-axis is shifted so that the centre of the heating at the time of the plots is always at $x = 0$ [Colour figure can be viewed at wileyonlinelibrary.com]

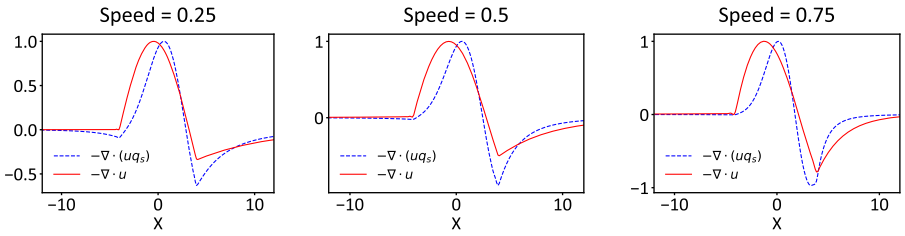

FIGURE 7 The velocity convergence and the humidity convergence at the Equator corresponding to three of the simulations (as labelled) in Figure 6. The humidity is the saturated value given by (3) using the height field of Figure 6 [Colour figure can be viewed at wileyonlinelibrary.com]

speed U. When $U = 0$ the equations exactly reproduce the Gill solution. The results (Figure 6) show that the pattern can maintain its coherence for values of U up to values of order c, the gravity wave speed, and at speeds above c the pattern in unsteady. It is the pressure field that is organizing the pattern and information is passed at a speed c, so the result is not surprising. Related results were obtained by Penn and Vallis (2017) in an exoplanet context and by Kacimi and Khouider (2018) in an MJO context. The eastward movement of the source does modify the pressure pattern, in particular by shortening the leading (eastward pointing) Kelvin lobe and (as is apparent in all but the resonant case when the source speed is one) lengthening the trailing Rossby lobes to something more of a swallowtail pattern, as might be expected since the source is moving in the same direction as the Kelvin waves.

For each of the height fields in Figure 6 we can calculate the saturation humidity using (3), and then calculate the convergence of that (i.e., $-\nabla\cdot(\mathbf{u}q_s)$). For speeds up to about three-quarters of the gravity wave speed ($0.75c$) where a Gill-like pattern can be clearly distinguished, the moisture convergence is to the east of velocity convergence (Figure 7). This speed provides an upper bound on the speed at which the MJO pattern may move. However, the gravity wave speed in Earth's tropical atmosphere is of order 20–30 $\mathrm{m\cdot s^{-1}}$ so that maintaining the coherence of a Gill-like pattern is evidently not the main determinant of the speed at which the MJO pattern can move (about 5 $\mathrm{m\cdot s^{-1}}$).

6.2 | Integrations with an interacting humidity field

We now evolve the humidity field alongside the usual shallow-water equations, with the precipitation of moisture providing a heat source in the height equation. However, we constrain the effects of the release of latent heat to occur only in a single prescribed region, distributed in a region surrounding the location of the condensation. We thereby eliminate the effects of all but a single condensing region, allowing for the potential formation and movement of an MJO-like event but preventing smaller-scale structures or grid-scale instabilities. We are thereby able to probe in a controlled fashion how the speed of propagation depends on the nature of the condensation and other parameters of the problem.

Typical solutions are shown in Figures 8 and 9. The equations are initially integrated for a period of time with a specified, stationary heat source centred at the Equator, representing a warm pool, with moisture treated as a passive tracer. The pressure field evolves into a Gill-like pattern and the associated velocity field converges moisture, producing precipitation east of the heat source, just

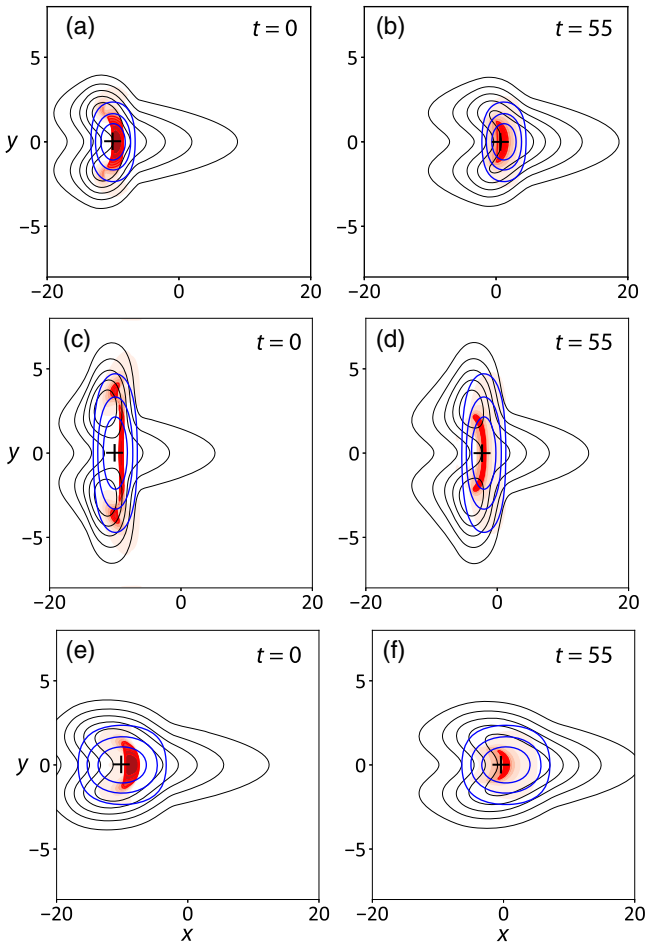

FIGURE 8 The pressure (zonally-elongated black contours), the moisture convergence ((red) shading) and the associated heating (blue contours surrounding the shading) at the non-dimensional times (a, c, e) 0 and (b, d, f) 55. The + indicates the centre of the velocity convergence. (a, c, e) show the fields with the heat source prescribed and stationary, with the precipitation then forming just east of that. The heat source is then allowed to respond to the position of the condensation, causing the pattern to translate east [Colour figure can be viewed at wileyonlinelibrary.com]

as in Figure 4. Once a steady state is reached, the heat source is allowed to follow the condensation, causing the pressure pattern to shift east. The moisture convergence and ensuing precipitation are also shifted east, and the entire system continues to propagate eastward. The peak of moisture convergence, precipitation and humidity itself are in all cases nearly coincidental, similar to the cases in Figure 4. Note, however, that we are not parametrizing the precipitation as a function of moisture convergence; rather, precipitation occurs on saturation.

In reality, an exact Gill pattern is not produced by latent heat release, and these results do not depend on that. To demonstrate this, we vary the shape of the condensational heat source, while still keeping its central position coincident with the peak of the condensation. In Figure 8a, b

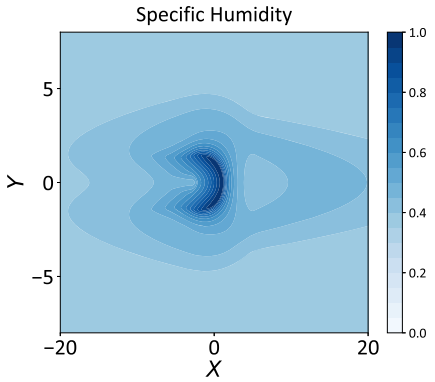

FIGURE 9 Snapshot of the specific humidity, scaled by its maximum value, in a numerical integration of the moist shallow-water equations. The pattern is moving eastward at a speed of about $0.2c$ or about $5\,\mathrm{m{\cdot}s^{-1}}$ [Colour figure can be viewed at wileyonlinelibrary.com]

the condensational heat source (blue contours) is specified to extend a few deformation radii both zonally and meridionally. In (c, d) the heating is extended meridionally, whereas in (e, f) the heating is extended zonally. The far field to the east is similar in all cases, since this is determined by the Kelvin wave response to the heat source at the Equator. The long 'fetch' brings in moisture ahead of the centre of the pattern, and eastward propagation occurs in all cases at speed of about $0.18c$, which if $c \approx 25\,\mathrm{m{\cdot}s^{-1}}$ is about $4.5\,\mathrm{m{\cdot}s^{-1}}$. This speed is determined in part by the strength of the condensation, which here is fixed and of such a strength as to produce fluid velocities that are also a few metres per second, as further explored below.

Note that initially, when the heat source is fixed independently of the moisture, the condensation is noticeably east of the heating source, just as in Figure 4. But once the heat source is taken to be at the location of the condensation, the pressure pattern can almost immediately catch up, because its response time, being set by the gravity wave speed, is shorter than the advective time-scale of the moisture. Thus, in all Figure 8a, c, e, condensation is noticeably east of the centre of the pattern, whereas in (b, d'f) the offset is smaller, consistent with the toy model result (7), that the offset is reduced by the ratio of the gravity wave speed to the fluid speed. Nonetheless, it is the fact that moisture converges toward the east of centre of the pressure pattern that enables the pattern to move eastward. The moisture is drawn in from the warm Kelvin lobe to the east but there are also meridional fluxes around the trailing Rossby lobes, as seen earlier in Figure 5. The difference between the moisture fluxes ($\mathbf{u}q$) and velocity itself ($\mathbf{u}$) is not very noticeable – it is the variation of the velocity field and not the moisture that is most responsible for the moisture convergence – but it is important.

6.3 | The speed of propagation

In the simple model of Section 5 the speed of propagation is proportional to the displacement, ΔX_C, and (in the relevant limit) the inverse time-scale, k_2. In the full equations the analogous two quantities are the displacement of the condensational latent heat release relative to the centre of the pressure pattern and the strength of the condensation heating; this latter quantity determines the velocity of the fluid that advects the humidity. Let us thus explore how the speed of propagation of the MJO depends on these quantities.

6.3.1 | The displacement

The eastward movement of the patterns shown in Figure 8 is produced by the slight offset between the location of the centre of the pattern (where the horizontal velocity itself converges) and the location of the latent heat release due to the precipitation. To obtain that figure a simple explicit representation of condensation was used, but various other representations of precipitation have been proposed, based for example on moisture convergence (Kuo, 1974) or column relative humidity (Bretherton *et al.*, 2004), and none can be presumed to be exact or necessarily appropriate in a given model. Furthermore, there is likely an adjustment and time lag between the condensation and its effect on the larger-scale flow. Accepting these uncertainties, we perform a sequence in which the condensational heat source used in the thermodynamic equation is displaced from the position of the moisture convergence (which is virtually coincident with the condensation) by varying amounts. (Note that we are not parametrizing the condensation by moisture convergence; the condensation is calculated using (2).) The strength of the heating is a constant, the same in each experiment, and is taken to extend a few deformation radii both zonally and horizontally, as in the blue contours in Figure 8a, b.

Figure 10 shows the results of these experiments, with a zero displacement corresponding to the heating coincident with the moisture convergence. As the specified displacement is increased, the propagation speed increases approximately linearly, as in the model of Section 5. This result does not depend on the exact specification of the heating structure and it holds in all the patterns shown in Figure 8.

6.3.2 | The disturbance amplitude

The disturbance amplitude is largely determined by the strength of the condensational heating; that is, the amplitude of Q_L in (1b)). In a sequence of experiments we vary the strength of this heating (keeping the strength fixed in each experiment) while allowing the model to determine the location of the region of condensation according to the equations of motion. The speed of propagation as a function of heating amplitude is shown in Figure 11. Unsurprisingly, the propagation speed increases with the disturbance amplitude, and is of a similar magnitude to the anomalous fluid velocity produced by the disturbance. The result arises because the fluid velocity determines the time-scale on which the moisture, the advected variable, can respond to changes in the pressure field, and that is the limiting factor in the adjustment of the whole pattern. For small values of the amplitude, the speed grows linearly with the amplitude before tapering off at large amplitude. At these large amplitudes the fluid speed is approaching that of the gravity wave speed so that the adjustment time of the pressure is no longer significantly shorter than that of the humidity. Similar behaviour is seen in the toy model (inset to Figure 11) when the parameter k_2 is varied, that parameter essentially representing and being proportional to a fluid velocity.

Evidently, at speeds lower than the gravity wave speed (which is the realistic regime) the propagation speed scales advectively, meaning it scales linearly with the fluid speed; the speed is limited by the advection of moisture and is not directly related to a gravity wave speed. The translation speed is similar to or somewhat greater than a typical fluid speed associated with the disturbance (and this is also the case in the observations, as noted later). It need not be thought of as a phase speed or group velocity associated with a wave, although it certainly may be possible to couch as such. Rather, it is the speed at which a coherent structure translates.

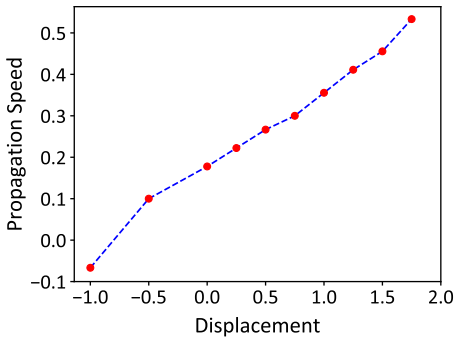

FIGURE 10 Speed of propagation of the MJO pattern as a function of the specified displacement of the condensational heating in the thermodynamic equation from the position of moisture convergence. Velocities are scaled with the gravity wave speed, c, and the displacement is scaled by the deformation radius [Colour figure can be viewed at wileyonlinelibrary.com]

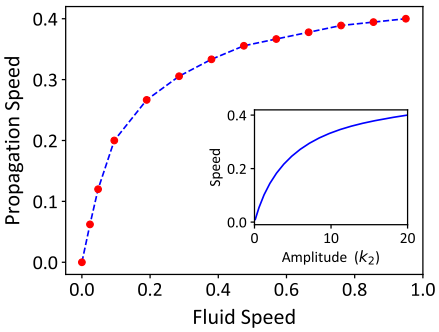

FIGURE 11 Speed of propagation of the MJO pattern as a function of rms fluid speed (which is directly proportional to the amplitude of the pattern). Values are non-dimensional, scaled with the gravity wave speed, c. The inset shows a corresponding plot for the toy model with speed given by (8), where k_2 is the inverse time-scale of the moisture convergence and $k_1 = 5$ and $\Delta x = 0.1$ [Colour figure can be viewed at wileyonlinelibrary.com]

6.4 | A self-consistent calculation of heating amplitude

Instead of specifying the amplitude of the condensational heating, we may suppose that it is (as in reality) proportional to the amount of precipitation multiplied by a latent heat of condensation. The moisture needed for the precipitation comes (in most part) from moisture convergence, and that in turn is determined by the amplitude of the condensational heating. Thus a feedback occurs, with more condensation leading to more convergence and hence more condensation. The ensuing instability is similar in some ways to that of Kuo (1975), although here all the fields remain in quasi-equilibrium (by construction). Other instabilities may play a role in real MJO events; for example, the moisture is ultimately supplied by evaporation from the surface, and that too will be enhanced if the flow is stronger.

To explore the effect of a self-consistent condensational heating calculation, we perform numerical experiments with, as before, the release of latent heat restricted to a single location spread over a region surrounding the location of condensation, but now with the heat source proportional to the amount of condensation. An MJO event is initiated by providing external heat source; then, as the instability grows, the latent heat release is allowed to take over as the source of heat. The disturbance becomes self-sustaining and begins to propagate eastward (not shown), with essentially the same mechanism, and the same resulting pattern, as that described above, provided that a dissipation mechanism (here a higher-order radiative damping on the height field) is present to prevent the instability from running away. The overall situation is similar to that described in Vallis and Penn (2020), although by restricting the heat source to a single region and prescribing its spatial extent, we prevent the formation of smaller outbreaks of convection and remove grid-point and time-step dependencies.

Although the underlying mechanism remains, as before, a simple one, there is some delicacy to the parameters that lead to a self-sustaining and propagating disturbance. For example, if the condensational heating is too weak, the disturbance never becomes self-sustaining and dies away, and if it is too strong the simulation can blow up. The heating depends on both the latent heat of condensation and the strength of the disturbance, and that in turn also depends on strength of the radiative damping and the efficiency of the evaporation. The propagation speed also depends on the location of the condensational heating and thus on the form of the precipitation parametrization. These sensitivities, and others, will also be present in more comprehensive model simulations. Thus, even if the mechanism itself is relatively simple, its reproduction in a model will not necessarily be so.

6.5 | Moisture as the only prognostic variable

It is possible to simply the model further (while still staying within the framework of the fluid equations of motion) by exploiting the fact that the pressure field responds more quickly to a change in forcing than does the moisture field. To this end we evolve the moisture field according to (4) and suppose that the pressure and velocity fields respond instantly to the diabatic heating arising from the precipitation, using the analytic form of the Gill solution or similar. The moisture convergence and precipitation is then calculated just as in the solutions shown above, but the system now has just one prognostic equation.

Solutions of this system (not shown) are very similar to those given above, and in particular the pattern propagates east at a similar speed to those shown. Using parameters that produce higher translation speeds, the solutions begin to differ in certain quantitative aspects because this model cannot capture the difference between the structure of a stationary Gill-like solution and a moving solution. Nonetheless, the essential mechanism of pattern formation and propagation is captured by such a model.

7 | OBSERVATIONS AND RELATED MODELS

7.1 | Observations

The overall patterns of the model presented above are broadly in accord with observations (and reanalyses) in

a number of respects, and in particular all of the listed features in Section 2 are accounted for. As many authors have pointed out, the general horizontal structure of the MJO has similarities with a GIll pattern. Here this is an unavoidable consequence of a localized heating centred around the Equator, caused by the latent heat released by the precipitation. It is this pattern that itself causes the moisture to converge, so sustaining the pattern. The actual solution will differ from a true Gill solution because of two effects: first, the MJO solution is moving, giving it somewhat longer trailing Rossby lobes; second, the distribution of latent heat release by the moisture is not in general the same as the heating in the original Gill problem. However, the far field does not care about the precise nature of the heating and neither of these effects is particularly large.

Observations do show that latent heat release is the dominant diabatic heating in the MJO system, producing anomalous velocities of a few metres per second (Jiang *et al.*, 2011; Adames and Wallace, 2015). Relatedly, observations show that moisture convergence, rather than local evaporation, is the primary supply of the precipitation in an MJO event (de Szoeke *et al.*, 2015). Evaporation is fairly constant over the warm equatorial region, whereas precipitation anomalies associated with the MJO are an order of magnitude larger than local evaporation anomalies. The moisture convergence arises both from zonal flow (with moist air coming in from the east along the Kelvin lobe) and meridionally, with flow around the trailing Rossby lobes, and mainly occurs in the lower atmosphere. In all these aspects the model is broadly consistent with observations.

A more stringent comparison arises by looking at the relative phases of pressure, velocity and moisture in the pattern as it propagates east. The moisture fluxes ($\mathbf{u}q$) are visually rather similar to the velocity vectors ($\mathbf{u}$), and the convergence is associated mainly with changes in velocity field rather than moisture itself, in both model and observations, with subtler differences accounting for the difference in their exact phase. Observation do show that convergence in the lower atmosphere increases moisture levels *ahead* of the convection (Jiang *et al.*, 2015; de Szoeke and Maloney, 2020). This offset is present in the model; in fact it is central to the eastward propagation. Enhanced convection to the east due to anomalous surface convergence associated with the Kelvin wave response and suppressed convection to the west was noted by Matthews (2000) and in fact suggested as a mechanism for eastward propagation. A similar effect was seen by Hsu and Li (2012) and is a key factor in some GCM simulations of the MJO (Hsu *et al.*, 2014). The notion of low-level convergence leading (i.e., being eastward of) the existing convection zone was also noted by Zhang and McPhaden (2000), Sperber (2003) and Maloney (2009), albeit with some differences of interpretation.

The eastward shift of precipitation relative to the centre of the pattern is key to the eastward propagation and is present in observations. But it should be said that observations (TRMM and GPCP) and reanalyses are not wholly in agreement as to the extent of the shift (Mapes and Bacmeister, 2012; Adames and Wallace, 2015). Results from the model suggest that eastward offset may be more evident in the early stages of the MJO, when the MJO is forming and the heating is in part due to a warm sea surface. Later in the cycle the moisture convergence and the velocity convergence are more nearly coincidental, as seen by comparing the right and left columns in Figure 8, because of the fast response of the pressure and velocity fields. Finally, we remark that the model does not seek to explain smaller-scale features of the MJO, such as the convective features surrounding the precipitating region. These arise in the numerical simulations of Vallis and Penn (2020), but are here regarded as inevitable consequences of the interaction of condensation and the pressure field rather than as an essential feature of the MJO itself.

7.2 | Related theories and models

The importance of the interaction between convection (and the latent heat release therein) and larger scale disturbances is an idea of long-standing going back to (at least) the CISK (conditional instability of the second kind) mechanism of Ooyama (1963; 1982), Charney and Eliassen (1964) and Kuo (1974). We do not explicitly invoke CISK in the sense of an instability drawing on the convective available potential energy (CAPE), and precipitation is not parametrized by a Kuo-type moisture convergence scheme. However, the convection does lead to the formation of a pressure perturbation in the form of Gill-like pattern extending over some thousands of kilometres. The associated moisture convergence then feeds and sustains the disturbance, and the east–west asymmetry of the moisture field gives rise to the slow quasi-static eastward propagation.

In some contrast to CISK, quasi-equilibrium ideas (Betts, 1973; Arakawa and Schubert, 1974; Emanuel *et al.*, 1994) argue that the role of convection is primarily to control the vertical temperature profile, keeping CAPE quasi-constant, rather that providing a heating. The large-scale flow remains in balance (i.e., in quasi-equilibrium) and it is this that allows the vertical structure to be constrained. Here, the use of the moist shallow-water equations may be regarded as a particularly severe form of quasi-equilibrium constraint. It is also

important to realize that quasi-equilibrium does not preclude the production of a large-scale response of the pressure field to convection, and the observation that a Gill-like pressure perturbation surrounds the region of precipitation in MJO events suggests that such a response does occur. An instability can arise because of that response, even if not strictly of CISK type.

As in the model presented here, 'moisture mode' theories rely on the response to condensation and the associated advection of moisture. In these theories (Majda and Stechmann, 2009; Raymond and Fuchs, 2009; Sobel and Maloney, 2013, and other articles by those authors) the eastward propagation of the MJO is generally associated with horizontal advection by anomalous lower-tropospheric winds resulting in an increase in humidity east of the enhanced convection and a drying west of the convection. However, there are differences both between the types of moisture-mode models themselves and with that presented here. In some of the Raymond–Fuchs models wind-induced evaporation was found essential in destabilizing the system and giving rise to propagation. Here, wind-induced evaporation plays no explicit role, although it was found to be a destabilizing feature in Vallis and Penn (2020) which enhanced the eastward propagation. The Sobel–Maloney model is one-dimensional and is highly parametrized, making certain assumptions as to the relation between precipitation and column water vapour, and radiative effects seem essential in destabilizing a column and maintaining the system. The model was extended to two dimensions by Adames and Kim (2016), and although they cast their results in terms of a dispersive wave, there are a number of similarities to the results here. In particular, their structure resembles a Gill-like response to an equatorial heat source, and moisture advection associated with the Rossby and Kelvin wave response leads to an eastward propagating moisture anomaly, similar in some ways to the description of Matthews (2000).

The 'trio interaction model' of Wang *et al.* (2016) uses a variant of the moist shallow-water equations and is presented as an integrative framework that includes moisture-mode and other theories. It has relatively elaborate parametrizations for physical processes – a cumulus parametrization, for example – and the authors couch their results in terms of an instability and a propagating mode. The resulting picture has similarities to that here and a Gill-like pattern emerges. The eastward propagation is ascribed to a variety of effects, including convective heating from the warm pool SST, the coupling of Kelvin and Rossby waves and the moisture feedback. In the model presented here, the warm pool (i.e., a stationary heat source) is only necessary for the MJO genesis. Once begun, the system is naturally self-sustaining and moisture feedback alone seems sufficient to provide propagation.

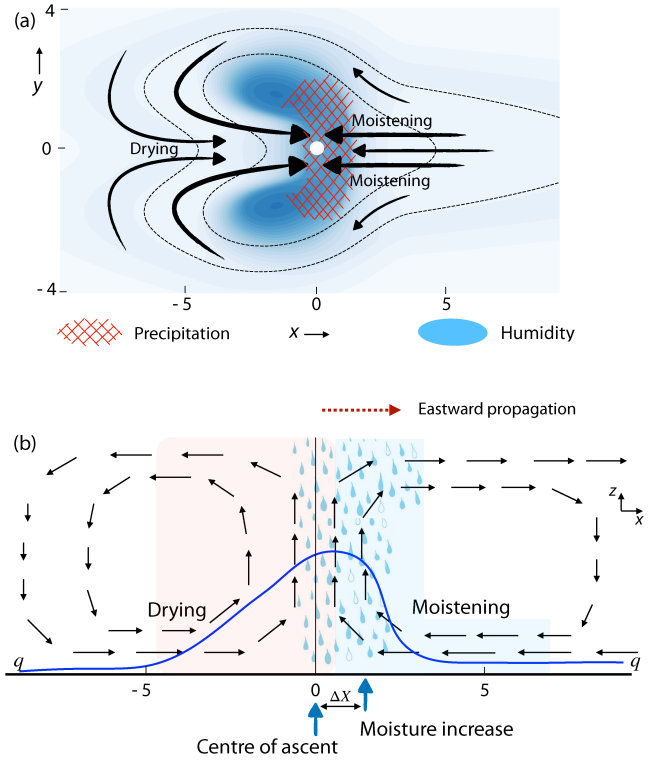

FIGURE 12 (a) Schematic of the horizontal structure of an idealized MJO, showing the main regions of moisture (blue shading), precipitation (red hatching), pressure (thin dashed contours) and velocity (arrows). The moistening and ensuing precipitation occurs a little east of the centre of the pattern (which is the white dot at (0, 0)), producing a pressure tendency that moves the pattern east. (b) Sketch of the corresponding vertical structure (in the x–z plane), with the solid blue curve at the bottom indicating the humidity levels in the lower atmosphere. As the pattern propagates east, the locations of precipitation and ascent become more nearly coincidental, but the process of moistening east of the disturbance remains [Colour figure can be viewed at wileyonlinelibrary.com]

The model presented by Vallis and Penn (2020) uses similar core equations to those presented here. It differs in that it allows a direct interaction with the moisture condensation and the pressure field; that is, condensation occurred immediately on saturation leading directly to heating. Various effects then come into play, including the dissipation, radiative destabilisation, the release of latent heat, and the presence or otherwise of wind-enhanced evaporation. However, the essential mechanism of eastward propagation is much the same as that presented here – namely moisture convergence and condensational heating occurring slightly to the east of the centre of the pattern, setting up a pressure field that pulls the pattern towards that heating. There was also an additional reason for the slight eastward offset: Kelvin waves emitted

by the convection propagate eastward, triggering more condensation east of the pattern centre.

The MJO performance of various general circulation models was evaluated by Jiang *et al.* (2015). Of particular note is their result that GCMs with a good MJO performance produced a low-level convergence and moisture accumulation east of the convection centre, whereas in those models that had a poor performance the convergence and enhanced rainfall were very close to the centre. This difference seems to arise from the much stronger Kelvin wave response in the good MJO models, although the differences in model physics which in turn give rise to that are not wholly clear. As an aside, Jiang *et al.* also found that cloud–radiative feedbacks were not of particular importance to good MJO performance.

It is clear that there are similarities and dissimilarities among these various approaches and models, with a common feature being moistening east of the disturbance. Here we have sought to give a phenomenological explanation of how that occurs and why it gives rise to eastward propagation. Additional theoretical work delineating the various commonalities and differences among models would be useful.

8 | CONCLUSIONS

This article has presented a model that gives rise to the structure of the MJO and exposes the mechanism of its eastward propagation in a transparent way, without attempting to be complete. The model suggests that the broad features of the three-dimensional structure of the MJO follow straightforwardly if latent heat release is a significant form of anomalous diabatic heating (as is observed). If this is concentrated around the Equator in a limited area then convective quasi-equilibrium gives rise to the observed vertical structure and a Gill-like pattern emerges in the horizontal. The issue then is why it moves eastward.

To understand that movement, consider that an MJO event may be initiated by heating from a warm sea surface, initially creating the Gill-like pattern. That pattern then converges moisture toward its centre, with the ensuing condensation sustaining the structure. However, the resulting east–west asymmetry of the pattern leads to the condensation occurring slightly to the east of the pattern's centre; this provides a new heat source east of the original one and eastward propagation is then unavoidable. Once propagating, the precipitation and the centre of the pattern are more nearly coincidental, as the pressure field responds quickly to the condensational heat source. The offset between the centre of the pattern and the precipitation may thus not be observationally detectable once the pattern has begun to progress; however, there will still be a detectable moistening tendency east of the centre of the pattern and this will be a signature of the mechanism. The two-dimensional structure (as in Figure 12a) is an essential aspect of this, and its presence allows the phenomenon to be reproduced in a model with only a few, relatively simple, physical parametrizations.

The mechanism described above is relatively simple. However, in reality there are many complications that both make a quantitative and closed mathematical theory (in the usual sense) impossible, and that make it difficult for comprehensive models to consistently reproduce the phenomena. Perhaps the most serious of these is the representation of precipitation and consequent release of latent heat, for these cannot be parametrized without making additional assumptions. Here we have explicitly accepted this limitation and assumed only that the latent heat is released in a coherent region surrounding the condensation, where that is largely a consequence of the moisture convergence (which is treated explicitly). However, and more generally, the treatment of convection and the associated condensation will inevitably affect the ability of a three-dimensional model to reproduce an MJO. In a GCM, if the convective parametrization is too sensitive then convection will be triggered too readily and the coherence of the latent heat release could be lost, and no Gill-like pattern with moistening east of the pattern centre would ensue. On the other hand, if convection is too hard to trigger, then the pattern will not be self-sustaining and may simply peter out. In neither case would a robust MJO be produced, and Yano *et al.* (1995) document some of the sensitivity to this in a simpler model. Other physical effects may then become important and, for example, cloud radiative cooling seems to play an important role in some models, and wind-induced evaporation is essential in others. This does not mean that such effects should be considered as driving the phenomena. Rather, it means they may be important in maintaining the instabilities necessary to sustain the convection producing the phenomenon. In sum, although the mechanism for MJO genesis and eastward propagation may in principle be simple, the entirety of the phenomenon is complex and its reproduction may depend sensitively on parameters and parametrizations in all but the highest resolution models.

In this picture the genesis of an MJO event naturally occurs over a warm moist ocean, for here there is an external source of heating which can initiate the convection and the convergence. However, once started, the system is self-sustained and the velocity of propagation then depends on two main factors:

1. The strength of the disturbance, for this determines the moisture advection that sustains the pattern and limits

the propagation speed. Thus, the propagation speed scales with the speed of the fluid that is created by the pattern and is similar to that speed. Observations do show that the anomalous fluid velocity generated by an MJO event is up to a few metres per second, of the same order as the translation speed.

2. The offset between the centre of the pattern and the location to which moisture is drawn and condensation occurs. This depends not only on the production of a large-scale Gill-like pattern in the pressure field, for this determines the moisture convergence, but also on the smaller-scale production of rainfall from the humidity field.

We have not tried to present an all-encompassing theory, and the limitations of the model we have used (e.g., no explicit boundary layer, a very simple representation of radiation, etc.) are apparent. Nor is the mechanism for propagation necessarily different from that appearing in other models – it will be unavoidably present in some, especially those that treat moisture advection fully. Rather, we have tried to identify and isolate the mechanism and present it in a simple form, explainable in words.

ACKNOWLEDGEMENTS

I would like to thank Sally Lavender, Alison Stirling and Prince Xavier, all of the UK Met Office, for many conversations regarding both the difficulties and the usefulness of comprehensive three-dimensional models. I also thank two anonymous reviewers for their many constructive comments. The work was funded by NERC under the ParaCon project, and by the Newton Fund under the Weather and Climate Science for Services Partnership. The author declares no known conflict of interest.

ORCID

Geoffrey K. Vallis https://orcid.org/0000-0002-5971-8995

REFERENCES

Adames, Á.F. and Kim, D. (2016) The MJO as a dispersive, convectively coupled moisture wave: theory and observations. *Journal of the Atmospheric Sciences*, 73, 913–941.

Adames, Á.F. and Wallace, J.M. (2015) Three-dimensional structure and evolution of the moisture field in the MJO. *Journal of the Atmospheric Sciences*, 72, 3733–3754.

Arakawa, A. and Schubert, W.H. (1974) Interaction of a cumulus cloud ensemble with the large-scale environment, Part I. *Journal of the Atmospheric Sciences*, 31, 674–701.

Arnold, N.P. and Randall, D.A. (2015) Global-scale convective aggregation: implications for the Madden–Julian Oscillation. *Journal of Advances in Modeling Earth System*, 7, 1499–1518.

Betts, A.K. (1973) Non-precipitating convection and its parametrization. *Quarterly Journal of the Royal Meteorological Society*, 99, 178–196.

Bouchut, F., Lambaerts, J., Lapeyre, G. and Zeitlin, V. (2009) Fronts and nonlinear waves in a simplified shallow-water model of the atmosphere with moisture and convection. *Physics of Fluids*, 21, 116604.

Bretherton, C.S., Peters, M.E. and Back, L.E. (2004) Relationships between water vapor path and precipitation over the tropical oceans. *Journal of Climate*, 17, 1517–1528.

Charney, J.G. and Eliassen, A. (1964) On the growth of the hurricane depression. *Journal of the Atmospheric Sciences*, 21, 68–75.

de Szoeke, S.P., Edson, J.B., Marion, J.R., Fairall, C.W. and Bariteau, L. (2015) The MJO and air–sea interaction in TOGA COARE and DYNAMO. *Journal of Climate*, 28, 597–622.

de Szoeke, S.P. and Maloney, E.D. (2020) Atmospheric mixed layer convergence from observed MJO sea surface temperature anomalies. *Journal of Climate*, 33, 547–558.

DeMott, C.A., Klingaman, N.P. and Woolnough, S.J. (2015) Atmosphere–ocean coupled processes in the Madden–Julian Oscillation. *Reviews of Geophysics*, 53, 1099–1154.

Emanuel, K.A., Neelin, J.D. and Bretherton, C.S. (1994) On large-scale circulations in convecting atmospheres. *Quarterly Journal of the Royal Meteorological Society*, 120, 1111–1143.

Fuchs, Ž. and Raymond, D.J. (2017) A simple model of intraseasonal oscillations. *Journal of Advances in Modeling Earth System*, 9, 1195–1211.

Gill, A.E. (1980) Some simple solutions for heat-induced tropical circulation. *Quarterly Journal of the Royal Meteorological Society*, 106, 447–462.

Holloway, C.E. and Neelin, J.D. (2009) Moisture vertical structure, column water vapor, and tropical deep convection. *Journal of the Atmospheric Sciences*, 66, 1665–1683.

Holloway, C.E., Woolnough, S.J. and Lister, G.M. (2013) The effects of explicit versus parameterized convection on the MJO in a large-domain high-resolution tropical case study. Part I: characterization of large-scale organization and propagation. *Journal of the Atmospheric Sciences*, 70, 1342–1369.

Hsu, P.-C. and Li, T. (2012) Role of the boundary layer moisture asymmetry in causing the eastward propagation of the Madden–Julian Oscillation. *Journal of Climate*, 25, 4914–4931.

Hsu, P.-C., Li, T. and Murakami, H. (2014) Moisture asymmetry and MJO eastward propagation in an aquaplanet general circulation model. *Journal of Climate*, 27, 8747–8760.

Jiang, X., Waliser, D.E., Olson, W.S., Tao, W.-K., L'Ecuyer, T.S., Li, K.-F., Yung, Y.L., Shige, S., Lang, S. and Takayabu, Y.N. (2011) Vertical diabatic heating structure of the MJO: intercomparison between recent reanalyses and TRMM estimates. *Monthly Weather Review*, 139, 3208–3223.

Jiang, X., Waliser, D.E., Xavier, P.K., Petch, J., Klingaman, N.P., Woolnough, S.J., Guan, B., Bellon, G., Crueger, T., DeMott, C., Hannay, C., Lin, H., Hu, W., Kim, D., Lappen, C.-L., Lu, M.-M., Ma, H.-Y., Miyakawa, T., Ridout, J.A., Schubert, S.D., Scinocca, J., Seo, K.-H., Shindo, E., Song, X., Stan, C., Tseng, W.-L., Wang, W., Wu, T., Wu, X., Wyser, K., Zhang, G.J. and Zhu, H. (2015) Vertical structure and physical processes of the Madden–Julian Oscillation: exploring key model physics in climate simulations. *Journal of Geophysical Research; Atmospheres*, 120, 4718–4748.

Kacimi, A. and Khouider, B. (2018) The transient response to an equatorial heat source and its convergence to steady state: implications for MJO theory. *Climate Dynamics*, 50, 3315–3330.

Khairoutdinov, M.F. and Emanuel, K.A. (2018) Intraseasonal variability in a cloud-permitting near-global equatorial aquaplanet model. *Journal of the Atmospheric Sciences*, 75, 4337–4355.
Kiladis, G.N., Straub, K.H. and Haertel, P.T. (2005) Zonal and vertical structure of the Madden–Julian Oscillation. *Journal of the Atmospheric Sciences*, 62, 2790–2809.
Kuo, H.-L. (1974) Further studies of the parameterization of the influence of cumulus convection on large-scale flow. *Journal of the Atmospheric Sciences*, 31, 1232–1240.
Kuo, H.-L. (1975) Instability theory of large-scale disturbances in the tropics. *Journal of the Atmospheric Sciences*, 32, 2229–2245.
Lau, W.K.-M. and Waliser, D.E. (Eds.) (2012) *Intraseasonal Variability in the Atmosphere–Ocean Climate System* (2nd edition). Berlin: Springer.
Liu, P., Satoh, M., Wang, B., Fudeyasu, H., Nasuno, T., Li, T., Miura, H., Taniguchi, H., Masunaga, H., Fu, X. and Annamalai, H. (2009) An MJO simulated by the NICAM at 14- and 7-km resolutions. *Monthly Weather Review*, 137, 3254–3268.
Madden, R.A. and Julian, P.R. (1971) Detection of a 40–50 day oscillation in the zonal wind in the tropical Pacific. *Journal of the Atmospheric Sciences*, 28, 702–708.
Madden, R.A. and Julian, P.R. (1972) Description of global-scale circulation cells in the tropics with a 40–50 day period. *Journal of the Atmospheric Sciences*, 29, 1109–1123.
Majda, A.J. and Stechmann, S.N. (2009) The skeleton of tropical intraseasonal oscillations. *Proceedings of the National Academy of Sciences*, 106, 8417–8422.
Maloney, E.D. (2009) The moist static energy budget of a composite tropical intraseasonal oscillation in a climate model. *Journal of Climate*, 22, 711–729.
Mapes, B.E. and Bacmeister, J.T. (2012) Diagnosis of tropical biases and the MJO from patterns in the MERRA analysis tendency fields. *Journal of Climate*, 25, 6202–6214.
Matsuno, T. (1966) Quasi-geostrophic motions in the equatorial area. *Journal of the Meteorological Society of Japan*, 44, 25–43.
Matthews, A.J. (2000) Propagation mechanisms for the Madden–Julian Oscillation. *Quarterly Journal of the Royal Meteorological Society*, 126, 2637–2651.
McCreary, J.P. (1981) A linear stratified ocean model of the equatorial undercurrent. *Philosophical Transactions of the Royal Society of London*, A298, 603–635.
Nasuno, T., Miura, H., Satoh, M., Noda, A.T. and Oouchi, K. (2009) Multi-scale organization of convection in a global numerical simulation of the December 2006 MJO event using explicit moist processes. *Journal of the Meteorological Society of Japan*, 87, 335–345.
Ooyama, K.V. (1963) *A Dynamical Model for the Study of Tropical Cyclone Development*. New York University. unpublished manuscript.
Ooyama, K.V. (1982) Conceptual evolution of the theory and modeling of the tropical cyclone. *Journal of the Meteorological Society of Japan*, 60, 369–380.
Penn, J. and Vallis, G.K. (2017) The thermal phase curve offset on tidally and non-tidally locked exoplanets: a shallow-water model. *The Astrophysical Journal*, 842, 101.
Raymond, D.J. and Fuchs, Ž. (2009) Moisture modes and the Madden–Julian Oscillation. *Journal of Climate*, 22, 3031–3046.
Sobel, A. and Maloney, E. (2013) Moisture modes and the eastward propagation of the MJO. *Journal of the Atmospheric Sciences*, 70, 187–192.
Sperber, K.R. (2003) Propagation and the vertical structure of the Madden–Julian Oscillation. *Monthly Weather Review*, 131, 3018–3037.
Sukhatme, J. (2014) Low-frequency modes in an equatorial shallow-water model with moisture gradients. *Quarterly Journal of the Royal Meteorological Society*, 140, 1838–1846.
Vallis, G.K. (2017) *Atmospheric and Oceanic Fluid Dynamics* (2nd edition). Cambridge, UK: Cambridge University Press.
Vallis, G.K. and Penn, J. (2020) Convective organization and eastward propagating equatorial disturbances in a simple excitable system. *Quarterly Journal of the Royal Meteorological Society*, 146, 2297–2314.
Wang, B., Liu, F. and Chen, G. (2016) A trio-interaction theory for Madden–Julian Oscillation. *Geoscience Letters*, 3, 1–16.
Wheeler, M. and Kiladis, G.N. (1999) Convectively coupled equatorial waves: analysis of clouds and temperature in the wavenumber–frequency domain. *Journal of the Atmospheric Sciences*, 56, 374–399.
Wheeler, M.C. and Hendon, H.H. (2004) An all-season real-time multivariate MJO index: development of an index for monitoring and prediction. *Monthly Weather Review*, 132, 1917–1932.
Yano, J.-I., McWilliams, J.C., Moncrieff, M.W. and Emanuel, K.A. (1995) Hierarchical tropical cloud systems in an analog shallow-water model. *Journal of the Atmospheric Sciences*, 52, 1723–1742.
Zhang, C. (2005) Madden–Julian Oscillation. *Reviews of Geophysics*, 43, 1–36.
Zhang, C. and McPhaden, M.J. (2000) Intraseasonal surface cooling in the equatorial western Pacific. *Journal of Climate*, 13, 2261–2276.

How to cite this article: Vallis, G.K. (2021) Distilling the mechanism for the Madden–Julian Oscillation into a simple translating structure. *Quarterly Journal of the Royal Meteorological Society*, 1–16. Available from: https://doi.org/10.1002/qj.4114

APPENDIX A

For reference, the geopotential in the Gill solution is (mostly using the notation of Vallis (2017) and in non-dimensional form with velocities scaled by c and lengths by L_d):

$$\phi_G = \frac{1}{2}\left[q_0(x) + q_2(x)(y^2+1)\right] \mathrm{e}^{-y^2/4}, \tag{A1}$$

where

$$q_0 = \begin{cases} \frac{-Ak}{r^2+k^2}\left(1+\mathrm{e}^{-2rL}\right)\mathrm{e}^{r(L-x)}, & x > L, \\ \frac{-A}{r^2+k^2}[r\cos kx & \\ \quad + k\left(\sin kx + \mathrm{e}^{-r(x+L)}\right)], & |x| < L, \\ 0, & x < -L, \end{cases} \tag{A2}$$

and

$$q_2 = \begin{cases} 0, & x > L, \\ \frac{A}{(3r)^2+k^2}[-3r\cos kx & \\ \quad + k\left(\sin kx - \mathrm{e}^{3r(x-L)}\right)], & |x| < L, \\ \frac{-Ak}{(3r)^2+k^2}\left[1+\mathrm{e}^{-6rL}\right]\mathrm{e}^{3r(x+L)}, & x < -L. \end{cases} \tag{A3}$$

Here, A is the amplitude of the forcing of the geopotential equation and which has the form $A\cos(kx)\exp(-y^2/4)$, $k = \pi/2L$. L is the prescribed zonal scale of the forcing (scaled by L_d), and r is a damping rate. Gill (1980) or Vallis (2017) give more detail. The saturated value of humidity may be evaluated by using (5) in conjunction with (A1), and the humidity convergence may then be evaluated using the associated expressions for the velocity field. Analytic expressions may in principle be obtained, but would still need to be evaluated numerically.